How close to detailed spectral calculations is the k-distribution method and correlated-k approximation of Kato et al. (1999) in each spectral interval?

William Wandji Nyamsi, Bella Espinar, Philippe Blanc, Lucien Wald

Meteorologische Zeitschrift, Vol. 23, No. 5, 547–556 (published online December 10, 2014)

How close to detailed spectral calculations is the k-distribution method and correlated-k approximation of Kato et al. (1999) in each spectral interval?

William Wandji Nyamsi*, Bella Espinar, Philippe Blanc and Lucien Wald

MINES ParisTech, PSL Research University, O.I.E. – Centre Observation, Impacts, Energy, Sophia Antipolis Cedex, France.

(Manuscript received April 12, 2014; in revised form August 1, 2014; accepted August 7, 2014)

Abstract

The k-distribution method and the correlated-k approximation of Kato et al. (1999) is a smart approach originally designed for broadband calculations of the solar radiation at ground level by dividing the solar spectrum in 32 spectral bands. The approach is a priori not suited for calculation of spectral irradiance. Nevertheless, this paper evaluates its performance when compared to more detailed spectral calculations serving as references for the spectral intervals no. 3 [283, 307] nm to 26 [1613, 1965] nm for clear and cloudy situations. The evaluation is based on numerical simulations. The clearer the sky, the greater the root mean square error (RMSE) in all bands. In the spectral intervals no. 3 and 4 [307, 328] nm, the irradiance is underestimated by large – approximately −90 % and −17 % in relative value - because the wavelength interval is large with respect to the absorption by ozone and a single value of ozone cross section is not enough for each interval. For each spectral interval from no. 5 [328, 363] nm to no. 18 [743, 791] nm, and for both global and direct radiation, the bias and the RMSE are less than 1.5 % of the irradiance in the corresponding interval under clear skies and may amount to 3 % in cloudy conditions. For greater wavelength intervals no. 19 to no. 26, the relative bias and RMSE show a tendency to increase with wavelength and may reach 8 % and 7 % for global and direct under clear skies respectively, and 11 % and 15 % under cloudy skies.

Keywords: absorption cross section, clear sky atmosphere, cloud, correlated-k approximation, spectral distribution of solar radiation

1 Introduction

The downwelling solar irradiance observed at ground level on horizontal surfaces and integrated over the whole spectrum (total irradiance) is called surface solar irradiance (SSI). It is an essential variable in many domains: climate, energy production, weather, oceanography, agriculture .... One may consider the total SSI, i.e. integrated over the solar spectrum or spectrally defined SSI. The global SSI is the sum of the direct SSI originating from the direction of the sun and of the diffuse SSI coming from the rest of the sky vault. Estimates of total SSI -global, direct and diffuse- are made by taking into account the various interactions between the solar radiation on its way downward and the atmospheric constituents. One of the difficulties in the computation lies in taking into account the gaseous absorption cross sections that are highly wavelength dependent. The best estimate is made by a calculation of the radiative transfer for each wavelength followed by integration over the solar spectrum. Such line-by-line calculations are computationally expensive.

Several methods have been proposed to reduce the number of calculations. Among them, are the k-distribution method and the correlated-k approximation proposed by Kato et al. (1999). It uses 32 wavelength intervals across the solar spectrum only to estimate the total SSI. The Kato et al. method is implemented in several Radiative Transfer Models (RTM) and reveals a very efficient way to speed up calculations of the total SSI. The goal of this article is to assess the potentials of the 32 estimates of SSI made in these intervals in order to provide a description of the spectral distribution of the SSI.

More exactly, the work studies how close to detailed calculations in each of these intervals are the estimates made by the Kato et al. method. If close enough, then this method could be exploited to help in calculating the SSI in specific spectral intervals. Ultraviolet (UV) radiation, daylighting, Photosynthetically Active Radiation (PAR), and spectral response of photovoltaic panels are examples of such specific intervals in various domains. The work focuses on the bands no. 3 to 26, i.e. from 283 to 1965 nm which is well representative of UV, PAR, visible band and all intervals related to common solar cells. The ozone present in the atmosphere extinguishes the solar radiation in the Kato bands no. 1 [240, 272] nm and no. 2 [272, 283] nm and the SSI is null at these wavelengths.

*Corresponding author: William Wandji Nyamsi, MINES ParisTech, PSL Research University, O.I.E. – Centre Observation, Impacts, Energy, CS 10207 rue Claude Daunesse, 06904 Sophia Antipolis Cedex, France, e-mail: william.wandji@mines-paristech.fr

DOI 10.1127/metz/2014/0607

Gebrüder Borntraeger Science Publishers, Stuttgart, www.borntraeger-cramer.com

The paper presents an overview of the KATO et al. method. For each spectral interval, estimates made by the KATO et al. method and by detailed calculations are compared for a wide range of atmospheric conditions. Both clear and cloudy skies are studied. Detailed spectral calculations are made with the RTMs libRadtran and SMARTS.

2 Overview of the *k*-distribution method and correlated-*k* approximation of KATO et al. (1999)

The *k*-distribution method is a technique of grouping wavelength intervals with similar spectral properties with k representing the gaseous absorption coefficient (WEST et al., 2010). In a homogeneous atmosphere, spectral transmittance is independent of the ordering of k for a given spectral interval and depends only on the fraction of the interval that is associated with a particular value of k (FU and LIOU, 1992). Hence, wavenumber integration may be replaced by integration over the k-space and more precisely by considering the probability of occurrence of a specific value of k in a wavelength interval through its cumulative distribution function (LIOU, 2002). In order to apply the *k*-distribution method to realistic atmospheres, variation in the absorption coefficient in the vertical must be accounted for. The correlated-*k* approximation assumes that the absorption cross section at a given wavelength always resides in the same interval of the cumulative distribution function, regardless of variations in total pressure, temperature and concentration (KATO et al. 1999).

Focusing on the calculation of the shortwave solar spectrum, from 240 nm to 4606 nm, KATO et al. (1999) have proposed a series of tables of absorption cross sections for water vapor, including continuum absorption, ozone, oxygen and carbon dioxide for 32 wavelength intervals, hereafter named "Kato bands" (KBs). Fig. 1 exhibits the distribution of the global spectral irradiance for a typical clear atmosphere (ASTM, 2003) in the 32 intervals and their corresponding relative contribution to the total irradiance. Table 1 lists the 32 spectral intervals.

The series of tables have been built in order to be integrated into RTMs to compute the total SSI in cloudy and clear sky conditions. KATO et al. (1999) found that the direct SSI computed by their approximation combined with a two-stream model for the mid-latitude summer standard atmosphere without aerosol in the clear sky conditions differs by 0.2 % or 2.1 $\mathrm{Wm^{-2}}$ from the result of the RTM MODTRAN3. Other authors have assessed this approximation. HALTHORE et al. (2005) presented a comparison of sixteen RTMs in which the RAPRAD one was using the approximation of KATO et al. (1999). Using the same RTM RAPRAD and same approximation, MICHALSKY et al. (2006) found that the relative error is less than 1 % and 1.9 % in respectively direct and diffuse total SSI under clear skies when comparing to measurements made during the ARM 2003 Aerosol Intensive Observation Period. These authors suggested that tests should be performed in the different portions of the spectrum for ensuring that cancellation errors are not responsible of this excellent performance. WANG et al. (2009) performed a comparison between the RTM DAK in combination with the approximation of KATO et al. (1999) and measurements in clear sky conditions. They found a bias of 2 $\mathrm{Wm^{-2}}$ (+0.2 %), 1 $\mathrm{Wm^{-2}}$ (+0.8 %) and 2 $\mathrm{Wm^{-2}}$ (+0.3 %) for respectively the direct, diffuse and global total SSI.

3 The RTMs used and their inputs

The present study is a pure modeling assessment. It is performed with the RTM libRadtran version 1.7 (MAYER and KYLLING, 2005; MAYER et al., 2012). In addition, the RTM SMARTS version 2.9.5 (Simple Model of the Atmospheric Radiative Transfer of Sunshine, GUEYMARD, 1995) is used to check that conclusions do not depend on this RTM and the aerosol model. SMARTS is limited to clear sky conditions. These two RTMs provide spectral irradiances and have been chosen because several articles have demonstrated the quality of their results when compared to spectral measurements.

The libRadtran (library for Radiative transfer) package software is a convenient set of tools for calculating radiative transfer in the Earth atmosphere. The main tool *uvspec* includes both the correlated-*k* approximation of KATO et al. (1999) and the pseudo-spectral calculations of the RTM SBDART. The correlated-*k* approximation uses the HITRAN molecular spectroscopic database. The pseudo-spectral calculations use the parameterization of absorption cross sections from LOWTRAN. The DISORT 2.0 (discrete ordinate technique) algorithm (STAMNES et al., 2000) was selected to solve the radiative transfer equation in both cases. Here, libRadtran is used twice: one in order to produce the spectral SSI in each Kato band, the second to produce detailed spectral calculations in each band serving as reference for the comparison.

The inputs to libRadtran governing the optical state of the clear atmosphere are the total column contents in ozone and water vapour, the vertical profile of temperature, pressure, density, and volume mixing ratio for gases as a function of altitude, the aerosol optical depth at 550 nm, Angström coefficient, and aerosol type, and the elevation of the ground above sea level. libRatran includes the recent aerosols models of the OPAC library of HESS et al. (1998). The set of additional inputs for the cloudy atmosphere comprises the cloud optical depth at 550 nm, the cloud phase, and the vertical position of the cloud. Default values in libRadtran for cloud liquid content and droplet effective radius are used: 1.0 $\mathrm{g\,m^{-3}}$ and 10 µm for water cloud, and 0.005 $\mathrm{g\,m^{-3}}$ and 20 µm for ice cloud. Solar spectrum of GUEYMARD (2004) was selected. Other inputs to libRadtran are the solar zenith angle Θ_s and the ground albedo ρ_g.

The inputs to SMARTS are the same than those to libRadtran. An exception is that only the aerosol optical

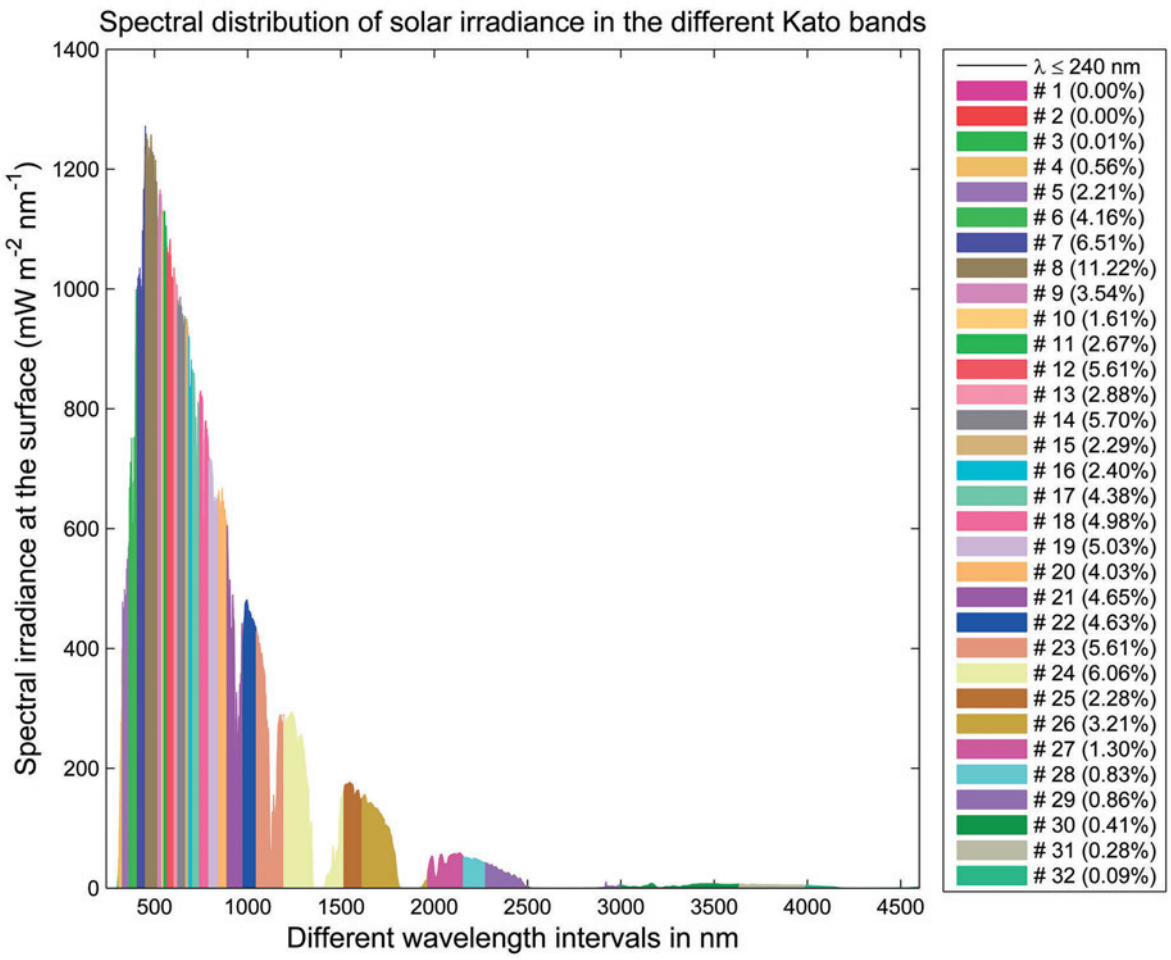

Figure 1: Example of distribution of the global spectral irradiance at surface in the 32 wavelength intervals of Kato et al. (1999) and their corresponding relative contribution in brackets to the total irradiance. Selected conditions are similar to ASTM (2003): solar zenith angle of 48.19 °, US standard atmosphere, total column contents in ozone of 343.8 DU and water vapor of 14.16 kg m^{-2}, aerosol rural type with an optical depth at 500 nm of 0.084 and an Angstrom exponent of 1.3, spectrally constant ground reflectance of 0.2.

Table 1: The spectral intervals selected by Kato et al. (1999)

Band number	Wavelength interval (μm)	Band number	Wavelength interval (μm)	Band number	Wavelength interval (μm)
1	[0.240, 0.272]	12	[0.567, 0.605]	23	[1.046, 1.194]
2	[0.272, 0.283]	13	[0.605, 0.625]	24	[1.194, 1.516]
3	[0.283, 0.307]	14	[0.625, 0.667]	25	[1.516, 1.613]
4	[0.307, 0.328]	15	[0.667, 0.684]	26	[1.613, 1.965]
5	[0.328, 0.363]	16	[0.684, 0.704]	27	[1.965, 2.153]
6	[0.363, 0.408]	17	[0.704, 0.743]	28	[2.153, 2.275]
7	[0.408, 0.452]	18	[0.743, 0.791]	20	[2.275, 3.001]
8	[0.452, 0.518]	19	[0.791, 0.844]	30	[3.001, 3.635]
9	[0.518, 0.540]	20	[0.844, 0.889]	31	[3.635, 3.991]
10	[0.540, 0.550]	21	[0.889, 0.975]	32	[3.991, 4.606]
11	[0.550, 0.567]	22	[0.975, 1.046]		

depth at 550 nm and the aerosol type are requested. SMARTS computes automatically the parameters (α, β) of the Angström relationship for two spectral ranges, below and above 500 nm. In order to ensure an exact comparison, libRadtran is forced to use the same values α and β and the aerosol model of Shettle (1989) used in SMARTS in case of clear sky conditions.

4 Method

The method is of statistical nature. Several sets of inputs to the RTMs are randomly built by a Monte-Carlo technique. Each set is input to libRadtran and to SMARTS for clear sky conditions only. For each set, two runs of libRadtran are made: one with the correlated-*k* approx-

imation of Kato et al. (1999) and the other with the pseudo-spectral calculation which serves as a reference. For each set and each Kato band, the differences between the estimates of the direct and global SSI made by respectively the correlated-k approximation and the pseudo-spectral calculation, and SMARTS in clear sky cases, are computed.

Table 2 reports the range of values taken respectively by Θ_s, ρ_g, and the variables describing the clear sky atmosphere. For computational reasons, Θ_s is set to 0.01 °, respectively 89 ° instead of 0 °, resp. 90 °. The random selection of inputs listed in this Table takes into account the modelled marginal distribution established from observation proposed by Lefevre et al. (2013) and Oumbe et al. (2011). More precisely, the uniform distribution is chosen as a model for marginal probability for all parameters except aerosol optical thickness, Angstrom coefficient, and total column ozone. The chi-square distribution for aerosol optical thickness, the normal distribution for the Angstrom coefficient, and the beta distribution for total column ozone have been selected. The selection of these parametric probability density functions and their corresponding parameters have been empirically determined from the analyses of the observations made in the AERONET network for aerosol properties and from meteorological satellite-based ozone products (Lefevre et al., 2013).

Ten randomly selected values of Θ_s and 10 values of ρ_g are combined with each of the 120 random selections of the other seven variables in Table 2, yielding a total of 12 000 clear atmospheric conditions that will be input to both libRadtran and SMARTS.

The cloud properties are associated together. Ranges of cloud optical depth are related to types of clouds to produce realistic conditions. Each selected cloud optical depth defines a series of 7 couples cloud base height-thickness for water clouds and 3 for ice clouds (Table 3). One thousand ($10 \times 10 \times 10$) combinations of Θ_s, ρ_g and cloud optical depth were generated. For each combination, 20 sets of the 7 clear sky variables were selected. To each cloud optical depth are associated 7 couples of cloud base height and thickness for water clouds and 3 for ice clouds, yielding a total of 140 000 atmospheric conditions for water clouds and 60 000 atmospheric conditions for ice clouds. Each condition was input to libRadtran.

In order to remove the daily and seasonal influence of the solar zenith angle on the SSI as well as the dependency to the extraterrestrial solar spectrum, the global SSI G_i estimated by the various models in the band KB i were converted into clearness index KT_i, also called atmospheric transmissivity, atmospheric transmittance, or atmospheric transmission:

$$KT_i = \frac{G_i}{E_{o_i}\cos(\Theta_s)} \tag{4.1}$$

where E_{o_i} is the irradiance at the top of atmosphere on a plane normal to the sun rays for the band KB i. Similarly, the direct clearness index KT_i^{dir} is defined as:

$$KT_i^{\mathrm{dir}} = \frac{B_i}{E_{o_i}\cos(\Theta_s)} \tag{4.2}$$

where B_i is the direct SSI.

For each set, the differences are computed on these indices. The differences are hereafter called errors as they quantify the errors made when using the approximation of Kato et al. (1999) instead of more detailed calculation of the SSI considered as reference for each spectral interval. The errors are synthesized by the bias, the root mean square error (RMSE), the squared correlation coefficient R^2, and by the bias (rBias) and RMSE (rRMSE) relative to the mean values of KT_i^{dir} and KT_i.

$$Bias = \frac{1}{n}\sum_{j=1}^{n} Y_{\mathrm{Estimated}(j)} - Y_{\mathrm{Reference}(j)} \tag{4.3}$$

$$RMSE = \sqrt{\frac{1}{n}\sum_{j=1}^{n}(Y_{\mathrm{Estimated}(j)} - Y_{\mathrm{Reference}(j)})^2} \tag{4.4}$$

$$rBias = \frac{100}{\overline{Y_{\mathrm{Reference}}}}Bias \tag{4.5}$$

$$rRMSE = \frac{100}{\overline{Y_{\mathrm{Reference}}}}RMSE \tag{4.6}$$

where j indicates each atmospheric state, n the total number of atmospheric states, the value Y can be KT, KT^{dir} for each KB and $\bar{Y}$ stands for the average value of Y. The reference value is the result from detailed spectral calculations of RTMs and the estimated value is that from the correlated-k approximation.

5 Results

5.1 Clear sky conditions

Fig. 2 is an example of scatterplot between spectrally detailed calculations (horizontal axis libRadtran and SMARTS) and the approximation of Kato et al. (1999) for the direct clearness index KT_i^{dir} for KB no. 9 [518, 540] nm. KT_i^{dir} is the main physical quantity used in the development of the correlated-k approximation. Points in the graph are well aligned along the 1:1 line with a very limited scattering. R^2 is greater than 0.999 which means that all information in the spectrally detailed calculations is explained by the correlated-k approximation for this band. The relative bias and RMSE are very small: respectively −0.4 % and 0.4 %. Results obtained with SMARTS are the same than for libRadtran. Findings are not surprising as this band exhibits a low molecular absorption. In this case, the values of k-distribution coefficient tables are sufficient to accurately model the attenuation of direct irradiance.

The approximation of Kato et al. does not perform so well for all intervals. Fig. 3 exhibits scatterplots for KB no. 3 [283, 307] nm and KB no. 4 [307, 328] nm.

Table 2: Range of values taken by the solar zenith angle, the ground albedo and the 7 variables describing the clear atmosphere

Variable	**Value**
Solar zenith angle Θ_s	0.01, 10, 20, 30, 40, 50, 60, 70, 80, 89 (degree)
Ground albedo ρ_g	0, 0.05, 0.1, 0.15, 0.2, 0.3, 0.4, 0.5, 0.7, 0.9
Total column content in ozone	Ozone content is: $300 * \beta + 200$, in Dobson unit. Beta distribution, with A parameter = 2, and B parameter = 2, to compute β
Total column content in water vapor	Uniform between 0 and 70 (k gm^{-2})
Elevation of the ground above mean sea level	Equiprobable in the set: 0, 1, 2, 3 (km)
Atmospheric profiles (Air Force Geophysics Laboratory standards)	Equiprobable in the set: Midlatitude Summer, Midlatitude Winter, Subarctic Summer, Subarctic Winter, Tropical, US. Standard
Aerosol optical depth at 550 nm	Gamma distribution, with shape parameter = 2, and scale parameter = 0.13
Angstrom coefficient *(only used with the OPAC library)*	Normal distribution, with mean = 1.3 and standard-deviation = 0.5
Aerosol type	Equiprobable in the set: urban, rural, maritime, tropospheric

Table 3: Selected cloud properties. Types of clouds and their acronyms; cumulus (Cu); stratocumulus (Sc); altostratus (As); altocumulus (Ac); cirrus (Ci) and cirrostratus (Cs).

Cloud optical depth	Water cloud (cloud base height + thickness, km)	Ice cloud (cloud base height + thickness, km)
0.5, 1, 2, 3 (and 4 for ice cloud only)	Cu: 0.4 + 0.2, 1 + 1.6, 1.2 + 0.2, 2 + 0.5 Ac: 2 + 3, 3.5 + 1.5, 4.5 + 1	Ci: 6 + 0.5, 8 + 0.3, 10 + 1
5, 7, 10, 20 (and 15 for ice cloud only)	Sc: 0.5 + 0.5, 1.5 + 0.6, 2 + 1, 2.5 + 2 As: 2 + 3, 3.5 + 2, 4.5 + 1	Cs: 6 + 0.5, 8 + 2, 10 + 1
40, 70	St: 0.2 + 0.5, 0.5 + 0.3, 1 + 0.5 Ns: 0.8 + 3, 1 + 1 Cb: 1 + 6, 2 + 8	–

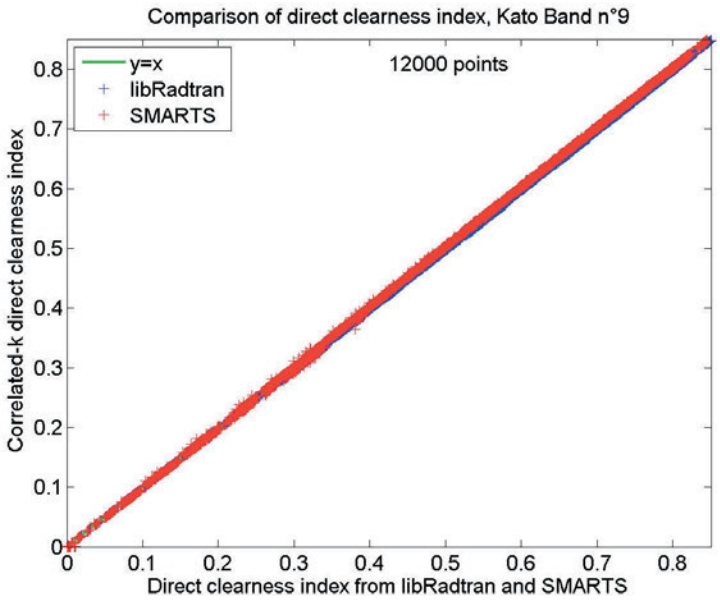

Figure 2: Scatterplot between spectrally detailed calculations (horizontal axis libRadtran and SMARTS) and the correlated-*k* approximation of Kato et al. (1999). Direct clearness index for KB no. 9 [518, 540] nm.

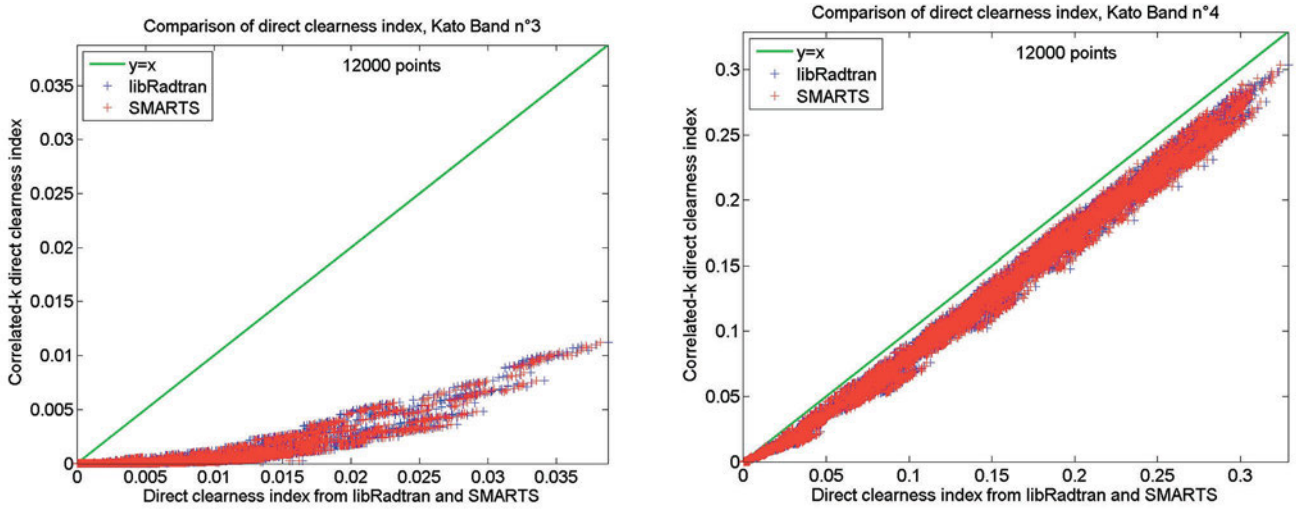

Figure 3: Scatterplot between spectrally detailed calculations (horizontal axis libRadtran and SMARTS) and the correlated-*k* approximation of Kato et al. (1999). Direct clearness index for KB no. 3 [283, 307] nm (left) and no. 4 [307, 328] nm (right).

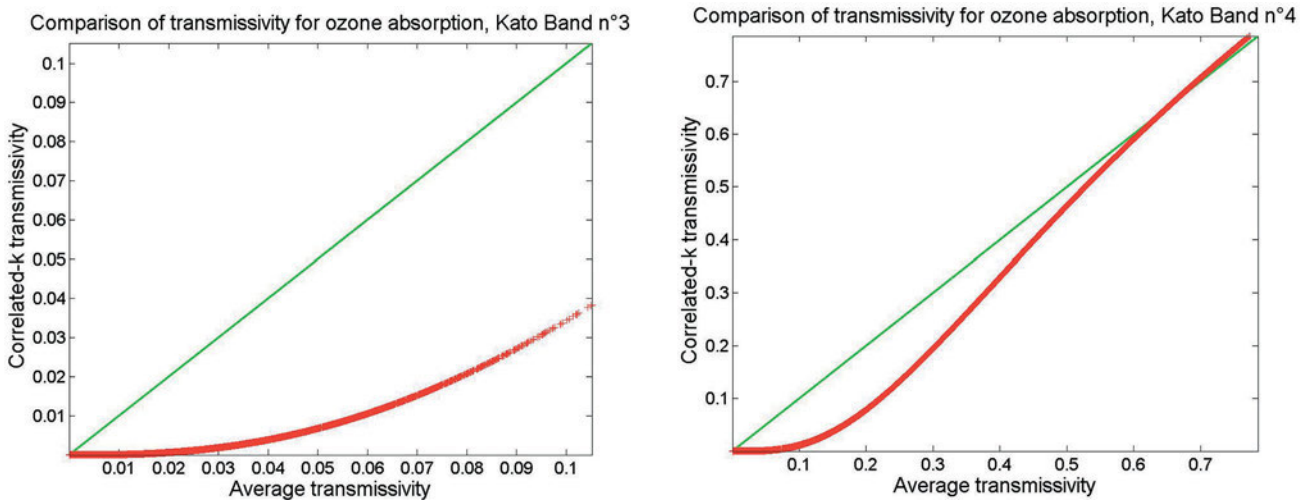

Figure 4: Scatterplots of transmissivity due only to ozone absorption between average by weighting with the extraterrestrial spectrum (horizontal axis) and the correlated-*k* approximation for KB no. 3 (left) and no. 4 (right).

For KB no. 3, the approximation strongly underestimates KT_i^{dir}. The relative bias is very large and amounts to −91.8 %. The scattering around the 1:1 line is nevertheless limited and R^2 is large: 0.677. The underestimation is less for KB no. 4: rBias is −13.9 %, rRMSE is 17.0 %. R^2 is very large: 0.995. The underestimation for these two bands can be explained by the fact that Kato et al. (1999) assume that the ozone cross section at the center wavelength in each interval represents the absorption over the whole interval. Actually, the ozone cross section is widely dependent of wavelength in this spectral region (Molina and Molina, 1986). The wavelength interval is large for considering only a single value of ozone cross section. Fig. 4 displays the comparison of transmissivities due only to ozone absorption between correlated-*k* approximation and average weighting with the extraterrestrial spectrum of Gueymard (2004) in KB no. 3 and 4. The behavior of the curves is similar to those in Fig. 3 and proves that the errors are mainly due by the choice made by Kato et al. for modelling ozone absorption.

Other KBs exhibit noticeable overestimation (no. 23, 24, 25) and underestimation (19, 21, 26). The water vapor is the main absorber in these wavelengths (Pierluissi and Peng, 1985). A part of uncertainties in the results is attributed to the different sources of spectroscopic data of Kato et al. method and detailed spectral calculations. Intervals KB 23 to 26 exhibit larger intervals than the previous ones. The influence of Θ_s, ground elevation, and as a whole of any variable that may influence the air mass is more visible. As an example, Fig. 5 exhibits the scatterplot between the libRadtran spectrally detailed calculations and the correlated-*k* approximation for two different ranges of solar zenith angle: $\Theta_s \leq 80\,^\circ$ and $\Theta_s = 89\,^\circ$ for KB no. 25. Errors are much larger at $\Theta_s = 89\,^\circ$ than at other Θ_s.

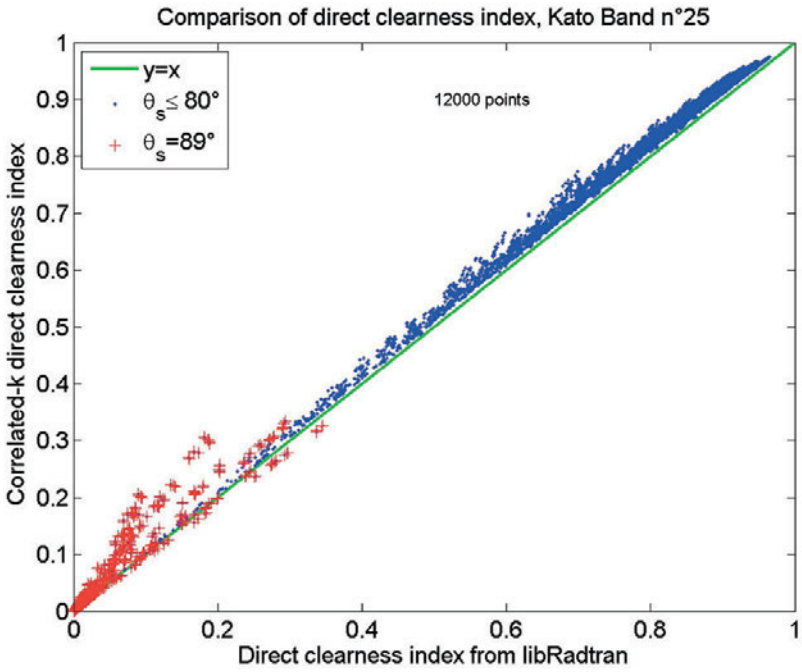

Figure 5: Scatterplot between libRadtran spectrally detailed calculations and the correlated-*k* approximation of Kato et al. (1999) for two ranges of solar zenith angle Θ_s. Direct clearness index for KB no. 25 [1516, 1613] nm.

Table 4 reports the statistical quantities summarizing the errors in KT_i^{dir} under clear sky conditions for $\Theta_s \leq 80\,^\circ$ with libRadtran calculations. One observes that R^2 is greater than 0.99 for all KBs from 4 to 26. All information in the spectrally detailed calculations is explained by the correlated-*k* approximation in each band, whatever the atmospheric profile, the aerosol model or other inputs. rBias ranges between a minimum of −6.8 % (KB no. 21) and a maximum of 6.0 % (KB no. 24). rRMSE amounts up to 7.4 %. In most KBs, rBias and rRMSE are less than 1.5 %. They are greater than 2.5 % in absolute value for KB no. 19, 21, 23, 24, 25 and 26. As already discussed, KB no. 3 and 4 are exceptions with large underestimation though R^2 is very large.

The results of errors in clearness index KT_i are summarized in Table 5 for $\Theta_s \leq 80\,^\circ$ with libRadtran calculations. For KB no. 3 and 4, rBias is respectively −92.2 % and −16.3 %, rRMSE is respectively 123.4 % and −16.9 %, and R^2 is respectively 0.718 and 0.991. rBias is small for most KBs. It ranges from −7.1 % (KB no. 21) to 5.3 % (KB no. 24). It is less than 1.5 % in absolute value for all bands, except KB no. 5, 19, 21, 23 and 26. Except KB no. 3 and 4, rRMSE is less than 2 % for the shortest wavelengths. It peaks at 7.6 % for KB no. 21 because of the large bias. As a whole, rRMSE is close to the absolute value of rBias, denoting a small standard-deviation of the errors. R^2 is very close to 0.99.

In general, rBias is greater for KT_i than for KT_i^{dir}. The global is the sum of the direct and diffuse components. The same correlated-*k* coefficient tables are used for each component, in the most KBs, leading to a larger error in the global than in the direct component.

5.2 Cloudy sky conditions

The results of errors in KT_i^{dir} and KT_i under cloudy skies are summarized in Tables 6–9 for $\Theta_s \leq 80\,^\circ$. Like clear sky conditions, errors for KB 3 and 4 are greater than for the other KB. For respectively $KT_i^{\mathrm{dir}}$and KT_i in KB no. 3, rBias is −90.7 % and −92.5 % for ice clouds and −91.5 % and −93.3 % for water clouds, rRMSE is approximately equal to the absolute value of rBias, and R^2 is 0.78 and 0.79 for ice clouds and 0.74 and 0.70 for water clouds. As for KB no. 4, rBias is −12.5 % and −16.8 % for ice clouds and −12.2 % and −16.0 % for water clouds, rRMSE is approximately equal to the absolute value of rBias, and R^2 is greater than 0.99.

Errors in KT_i^{dir} depend on the KB (Table 6–7) but do not depend noticeably on the cloud phase. rBias ranges between −6.2 % (KB no. 21) and 5.3 % (KB no. 24). rRMSE amounts up to 15.1 % for KB no. 21. In all KBs, except no. 21, rBias is much less than 5 % in absolute value. For most KBs, rRMSE is less than 5 %.

The errors in KT_i^{dir} in cloudy conditions slightly depend on the cloud optical depth and to a much lesser extent on the other cloud properties. They exhibit the same dependency than those for clear sky on Θ_s, ground elevation, and as a whole of any variable that may influence the air mass. R^2 is greater than 0.99 for all KBs from 4 to 26. All information in the spectrally detailed calculations is explained by the correlated-*k* approximation in each band, whatever the cloudy conditions, atmospheric profile, the aerosol model or other inputs.

The errors on KT_i depend on the KB (Table 8–9) and do not depend noticeably on the cloud phase, except for KB no. 24 and 26. rBias ranges between −7.4 %

Table 4: Statistical parameters in the different KBs for the direct clearness index under clear sky conditions for $\Theta_s \leq 80\,^\circ$ with libRadtran calculations. N° is the number of KB, R^2 is the squared correlation coefficient, Mean is the mean value of the index.

N°	R^2	Mean	rBias(%)	rRMSE(%)	N°	R^2	Mean	rBias(%)	rRMSE(%)
3	0.682	0.006	−91.8	132.2	15	0.999	0.665	−0.0	0.0
4	0.995	0.128	−13.9	16.1	16	0.999	0.616	−0.6	1.0
5	0.999	0.254	0.9	1.1	17	0.999	0.602	0.7	1.4
6	0.999	0.354	−1.0	1.0	18	0.999	0.666	0.9	1.3
7	0.999	0.435	−0.1	0.2	19	0.995	0.671	−2.5	3.1
8	0.999	0.506	0.3	0.3	20	0.999	0.753	0.5	0.6
9	0.999	0.546	−0.4	0.4	21	0.993	0.459	−6.8	7.4
10	0.999	0.556	−0.2	0.2	22	0.998	0.760	−0.2	1.0
11	0.999	0.561	−0.2	0.2	23	0.998	0.521	2.3	2.6
12	0.999	0.558	1.4	1.5	24	0.995	0.406	6.0	6.3
13	0.999	0.599	0.2	0.2	25	0.997	0.806	2.9	3.1
14	0.999	0.618	1.3	1.4	26	0.994	0.453	−3.1	3.7

Table 5: Statistical parameters in the different KBs for the clearness index under clear sky conditions for $\Theta_s \leq 80\,^\circ$ with libRadtran calculations. N° is the number of KB, R^2 is the squared correlation coefficient, Mean is the mean value of the index.

N°	R^2	Mean	rBias(%)	rRMSE(%)	N°	R^2	Mean	rBias(%)	rRMSE(%)
3	0.718	0.016	−92.8	123.4	15	0.999	0.895	−0.0	0.3
4	0.991	0.377	−16.3	16.9	16	0.997	0.815	−0.8	1.1
5	0.999	0.671	1.7	1.8	17	0.995	0.782	0.7	1.4
6	0.999	0.755	−0.2	0.2	18	0.994	0.853	1.1	1.5
7	0.999	0.806	−0.0	0.0	19	0.986	0.839	−2.7	3.3
8	0.999	0.837	0.1	0.1	20	0.999	0.932	0.5	0.6
9	0.999	0.840	−0.4	0.5	21	0.994	0.547	−7.1	7.5
10	0.999	0.834	−0.2	0.3	22	0.990	0.904	−0.2	1.1
11	0.999	0.831	−0.2	0.3	23	0.996	0.603	2.1	2.5
12	0.999	0.798	1.5	1.5	24	0.991	0.458	5.3	5.6
13	0.999	0.839	0.2	0.3	25	0.988	0.891	3.0	3.1
14	0.994	0.845	1.4	1.8	26	0.989	0.495	−3.6	4.0

Table 6: Statistical parameters in the different KBs for the direct clearness index under cloudy sky conditions for $\Theta_s \leq 80\,^\circ$ and ice cloud phase. N° is the number of KB, R^2 is the squared correlation coefficient, Mean is the mean value of the index.

N°	R^2	Mean	rBias(%)	rRMSE(%)	N°	R^2	Mean	rBias(%)	rRMSE(%)
3	0.783	0.001	−90.7	274.2	15	0.999	0.053	0.0	0.1
4	0.998	0.011	−12.5	31.2	16	0.999	0.050	−0.5	1.6
5	0.999	0.022	0.8	2.1	17	0.999	0.049	1.0	3.4
6	0.999	0.030	−1.0	2.2	18	0.999	0.053	0.8	1.9
7	0.999	0.037	−0.3	0.6	19	0.999	0.053	−1.8	5.3
8	0.999	0.042	0.2	0.6	20	0.999	0.059	0.4	1.0
9	0.999	0.045	−0.3	0.7	21	0.999	0.039	−5.8	14.3
10	0.999	0.046	−0.2	0.4	22	0.999	0.059	−0.3	1.6
11	0.999	0.046	−0.2	0.4	23	0.999	0.042	3.4	7.6
12	0.999	0.046	1.3	3.1	24	0.999	0.033	5.3	12.3
13	0.999	0.049	0.2	0.4	25	0.999	0.063	2.8	6.3
14	0.999	0.050	1.2	2.9	26	0.999	0.036	−3.8	9.0

(KB no. 21) and 10.1 % (KB no. 24). rRMSE is equal to the absolute value of rBias meaning that the standard-deviation of the errors is small. R^2 is greater than 0.99 for all KBs from no. 4 to 26. Like in the clear sky case, and for the same reasons, the errors are larger in the global than in the direct component in the most KBs.

The errors slightly depend on the cloud optical depth and to a much lesser extent on the ground albedo and other cloud properties. They exhibit the same dependency than those for clear sky on Θ_s, ground elevation, and as a whole of any variable that may influence the air mass.

Conclusion

The presented study demonstrates that as a whole the *k*-distribution method and the correlated-*k* approximation

Table 7: Statistical parameters in the different KBs for the direct clearness index under cloudy sky conditions for $\Theta_s \leq 80\,^\circ$ with water cloud phase. N° is the number of KB, R^2 is the squared correlation coefficient, Mean is the mean value of the index.

N°	R^2	Mean	rBias(%)	rRMSE(%)	N°	R^2	Mean	rBias(%)	rRMSE(%)
3	0.744	0.001	−91.5	279.7	15	0.999	0.055	0.0	0.1
4	0.998	0.012	−12.1	29.92	16	0.999	0.052	−0.3	1.4
5	0.999	0.023	0.6	1.9	17	0.999	0.051	0.9	3.1
6	0.999	0.032	−0.6	1.7	18	0.999	0.055	0.5	1.4
7	0.999	0.039	−0.2	0.4	19	0.995	0.055	−1.9	5.4
8	0.999	0.045	0.3	0.7	20	0.999	0.060	0.5	1.2
9	0.999	0.048	−0.3	0.7	21	0.993	0.040	−6.2	15.1
10	0.999	0.049	−0.1	0.3	22	0.998	0.061	0.2	1.7
11	0.999	0.049	−0.1	0.4	23	0.998	0.043	1.9	5.1
12	0.999	0.048	1.3	3.0	24	0.995	0.033	5.3	12.3
13	0.999	0.051	0.2	0.4	25	0.997	0.062	2.3	5.6
14	0.999	0.052	1.2	2.8	26	0.994	0.035	−4.2	10.2

Table 8: Statistical parameters in the different KBs for the clearness index under cloudy sky conditions for $\Theta_s \leq 80\,^\circ$ with ice cloud phase. N° is the number of KB, R^2 is the squared correlation coefficient, Mean is the mean value of the index.

N°	R^2	Mean	rBias(%)	rRMSE(%)	N°	R^2	Mean	rBias(%)	rRMSE(%)
3	0.794	0.011	−92.5	135.5	15	0.999	0.597	0.1	0.2
4	0.985	0.263	−16.8	18.2	16	0.999	0.537	−0.4	1.0
5	0.999	0.468	1.9	2.1	17	0.999	0.515	1.1	1.9
6	0.999	0.519	−0.2	0.2	18	0.999	0.564	1.6	2.0
7	0.999	0.550	−0.1	0.1	19	0.997	0.551	−2.1	2.9
8	0.999	0.566	0.1	0.2	20	0.999	0.616	0.9	1.1
9	0.999	0.566	−0.3	0.4	21	0.995	0.362	−6.7	7.5
10	0.999	0.564	−0.2	0.2	22	0.999	0.590	0.0	1.0
11	0.999	0.558	−0.1	0.3	23	0.999	0.394	3.1	3.7
12	0.999	0.533	2.0	2.3	24	0.992	0.280	10.2	11.2
13	0.999	0.563	0.3	0.4	25	0.999	0.392	2.8	3.7
14	0.999	0.562	1.8	2.0	26	0.999	0.223	−3.1	4.1

Table 9: Statistical parameters in the different KBs for the clearness index under cloudy sky conditions for $\Theta_s \leq 80\,^\circ$ with water cloud phase. N° is the number of KB, R^2 is the squared correlation coefficient, Mean is the mean value of the index.

N°	R^2	Mean	rBias(%)	rRMSE(%)	N°	R^2	Mean	rBias(%)	rRMSE(%)
3	0.695	0.011	−93.3	132.7	15	0.999	0.590	0.0	0.1
4	0.986	0.270	−15.9	17.6	16	0.999	0.532	−0.6	1.1
5	0.999	0.473	1.8	2.0	17	0.999	0.510	0.7	1.5
6	0.999	0.523	−0.1	0.2	18	0.999	0.557	1.4	1.7
7	0.999	0.552	−0.0	0.0	19	0.998	0.540	−2.5	3.2
8	0.999	0.567	0.1	0.1	20	0.999	0.602	0.7	0.9
9	0.999	0.566	−0.4	0.4	21	0.997	0.347	−7.4	8.3
10	0.999	0.564	−0.2	0.2	22	0.999	0.574	0.0	1.0
11	0.999	0.558	−0.1	0.2	23	0.999	0.374	2.0	2.7
12	0.999	0.531	1.8	2.0	24	0.998	0.269	3.4	5.8
13	0.999	0.558	0.3	0.3	25	0.999	0.486	3.1	3.8
14	0.999	0.557	1.6	1.8	26	0.999	0.259	−6.6	7

proposed by KATO et al. (1999) for several spectral intervals offer accurate estimates of the spectral irradiance in these intervals when compared to detailed spectral calculations in clear sky and cloudy conditions. The study is based on a pure modeling approach and is limited to the bands no. 3 to 26.

In all cases, whatever the spectral band, the greatest error is reached for clear sky conditions and decreases considerably as the extinction due to cloud increases. For spectral intervals from no. 5 [328, 363] nm to no. 18 [743, 791] nm, and for both global and direct radiation, the bias and the RMSE are less than 1.5 % of the irradiance in the corresponding interval under clear skies and may amount to 3 % in cloudy conditions. For spectral intervals no. 19 [791, 844] nm to 26 [1613, 1965] nm and in most case, the errors amount to less than 5 % of the irradiance in the corresponding interval for both global and direct radiation. The relative bias and RMSE show a

tendency to increase with wavelength for greater wavelength intervals and may reach 8 % and 7 % for global and direct under clear skies respectively, and 11 % and 15 % under cloudy skies.

The situation is not so good for the spectral intervals no. 3 [283, 307] nm and 4 [307, 328] nm. The irradiance is underestimated by large – approximately −90 % and −17 % in relative value – because the wavelength interval is large with respect to the absorption by ozone and a single value of ozone cross section is not enough for each interval. As a consequence, the approach is not directly useful for the ultraviolet radiation.

The present study has practical implication as it provides an assessment of the errors made when using the *k*-distribution method and the correlated-*k* approximation proposed by Kato et al. (1999) instead of more detailed calculations that are more demanding in computational resources.

Acknowledgements

The authors thank the teams developing libRadtran (http://www.libradtran.org) and SMARTS. They also thank S. Kato for encouraging them to undertake the study. This work was partly funded by the French Agency ADEME in charge of energy (grant no. 1105C0028, 2011–2016) and took place within the Task 46 "solar resource assessment and forecasting" of the Solar Heating and Cooling programme of the International Energy Agency

References

ASTM, 2003: "Standard tables for reference solar spectral irradiance at air mass 1.5: Direct normal and hemispherical for a 37 ° tilted surface," Standard G173-03. – American Society for Testing and Materials, West Conshohocken.

Fu, Q., K.-N. Liou, 1992: On the correlated *k*-distribution method for radiative transfer in nonhomogeneous atmosphere. – J. Atmos. Sci. **49**, 2139–2156, DOI: 10.1175/1520-0469(1992)049<2139:OTCDMF>2.0.CO;2.

Gueymard, C., 1995: SMARTS2, Simple model of the atmospheric radiative transfer of sunshine: algorithms and performance assessment. – Report FSEC-PF-270-95, Florida Solar Center, Cocoa, FL., USA, http://www.fsec.ucf.edu/en/publications/pdf/FSEC-PF-270-95.pdf

Gueymard, C., 2004: The sun's total and the spectral irradiance for solar energy applications and solar radiations models. – Solar Energy **76**, 423–452 DOI:10.1016/j.solener.2003.08.039

Halthore, R.N., D. Crisp, S.E. Schwartz, G.P. Anderson, A. Berk, B. Bonnel, O. Boucher, F.-L. Chang, M.-D. Chou, E.E. Clothiaux, P. Dubuisson, B. Fomin, Y. Fouquart, S. Freidenreich, C. Gautier, S. Kato, I. Laszlo, Z. Li, J.H. Mather, A. Plana-Fattori, V. Ramaswamy, P. Ricchiazzi, Y. Shiren, A. Trishchenko, W. Wiscombe, 2005: Intercomparison of shortwave radiative transfer codes and measurements. – J. Geophys. Res. **110**, D11206. DOI:10.1029/2004JD005293.

Hess, M., P. Koepke, I. Schult, 1998: Optical Properties of Aerosols and Clouds: The Software Package OPAC. – Bull. Amer. Meteor. Soc. **79**, 31–844, DOI: 10.1175/1520-0477(1998)079<0831:OPOAAC>2.0.CO;2.

Kato, S., T. Ackerman, J. Mather, E. Clothiaux, 1999: The *k*-distribution method and correlated-*k* approximation for shortwave radiative transfer model. – J. Quant Spectroscopy Radiative Transfer **62**, 109–121 DOI: 10.1016/S0022-4073(98)00075-2

Lefevre, M., A. Oumbe, P. Blanc, B. Espinar, B. Gschwind, Z. Qu, L. Wald, M. Schroedter-Homscheidt, C. Hoyer-Klick, A. Arola, A. Benedetti, J.W. Kaiser, J.-J. Morcrette, 2013: McClear: a new model estimating downwelling solar radiation at ground level in clear-sky conditions. – AMT **6**, 2403–2418, DOI:10.5194/amt-6-2403-2013.

Liou, K.-N., 2002: An Introduction to Atmospheric Radiation. – Int. Geophysics Series, Academic Press **84**, Second Edition, 583pp.

Mayer, B., A. Kylling, 2005: Technical note: The libRadtran software package for radiative transfer calculations-description and examples of use. – Atmos. Chem. Phys. **5**, 1855–1877, DOI:10.5194/acp-5-1855-2005.

Mayer, B., A. Kylling, C. Emde, U. Hamann, R. Buras, 2012: libRadtran user's guide. Edition for libRadtran. – Available at www.libradtran.org/doc/libRadtran.pdf.

Michalsky, J.J., G.P. Anderson, J. Barnard, J. Delamere, C. Gueymard, S. Kato, P. Kiedron, A. Mccomiskey, P. Ricchiazzi, 2006: Shortwave radiative closure studies from clear skies during the Atmospheric Radiation Measurement 2003 Aerosol Intensive Observation Period. – J. Geophys. Res. 111D, D14S90, DOI:10.1029/2005JD006341.

Molina, L.T., M.J. Molina, 1986: Absolute absorption cross sections of zone in the 185- to 350 nm wavelength range. – J Geophys. Res **91**, 14501–14508. DOI: 10.1029/JD091iD13p14501.

Oumbe, A., P. Blanc, B. Gschwind, M. Lefevre, Z. Qu, M. Schroedter-Homscheidt L. Wald, 2011: Solar irradiance in clear atmosphere: study of parameterisations of change with altitude. – Adv. Sci. Res. **6**, 199–203, DOI:10.5194/ASR-6-199-2011.

Pierluissi, J.H., G.-S. Peng, 1985: New molecular transmission band models for LOWTRAN. – Optical Engineering 24, 541–547, DOI:10.1117/12.7973523.

Shettle, E., 1989: Models of aerosols, clouds and precipitation for atmospheric propagation studies. – In: Atmospheric propagation in the UV, Visible, IR and MM-region and Related system aspects, no. 454 in AGARD Conference Proceedings.

Stamnes, K., S.-C. Tsay, W. Wiscombe, I. Laszlo, 2000: DISORT, a general purpose Fortran program for discrete ordinate method radiative transfer in scattering and emitting layered media: Documentation of methodology. – Tech. Rep., Dept. of Physics and Engineering Physics, Stevens Institute of Technology, Hoboken, NJ07030, USA.

Wang, P., W.H. Knap, P.K. Munneke, P. Stamnes, 2009: Clear-sky shortwave radiative closure for the Cabauw Baseline Surface Radiation Network site, Netherlands. – J. Geophys. Res. 114, D14206, DOI:10.1029/2009JD011978.

West, R., R. Goody, L. Chen, D. Crisp, 2010: The correlated-k method and related methods for broadband radiation calculations. – J. Quant. Spectros. Radiative Transfer 111, 1672–1673, DOI:10.1016/j.jqsrt.2010.01.013.